Research Square

Preprints are preliminary reports that have not undergone peer review.
They should not be considered conclusive, used to inform clinical practice,
or referenced by the media as validated information.

Orthorhombic crystal structured Dy3+ dopedLi2Cd2(PO4)2 nanopowders for yellowish light emitting solid state lighting applications

Shaik Azad Basha
Acharya Nagarjuna University
K. Srinivasarao
Govt. Degree College, Palakonda
K. Daniel
Dr. Samuel George Institute of Engineering and Technology
B.V. Naveen Kumar
University of Free state
Y. Nirmal Rajeev
Siddardha Academy of Higher Education
Prof. Sandhya Cole
sandhya.cole@gmail.com

Acharya Nagarjuna University

Research Article

Keywords: Li2Cd2(PO4)2, Photoluminescence, FESEM, Dexter's theory, PLQY, SSR method

Posted Date: May 8th, 2026

DOI: https://doi.org/10.21203/rs.3.rs-8763095/v1

License: This work is licensed under a Creative Commons Attribution 4.0 International License. Read Full License

Additional Declarations: No competing interests reported.

Version of Record: A version of this preprint was published at Chemical Papers on June 20th, 2026. See the published version at https://doi.org/10.1007/s11696-026-05178-6.

Abstract

Pure and Dy^{3+} doped lithium cadmium orthophosphate (LCP=$Li_2Cd_2(PO_4)_2$) nanopowders (NPs) were synthesized using the Solid-State Reaction (SSR) method. The XRD analysis revealed the orthorhombic crystal structure with Pnma space group. The W-H plot and Scherrer's methods were used to calculate the average crystallite size for both pure and Dy^{3+} doped LCP NPs. The elemental composition was verified by EDS analysis, and the clustered irregular stone-like structure was identified using FE-SEM analysis. Raman and FT-IR analyses were used to identify the $(PO_4)^{3-}$vibrational modes.The optical bandgap values of the pure, 0.01 mol% ($Dy_{0.01}$), 0.05 mol% ($Dy_{0.05}$) and 0.09 mol% ($Dy_{0.09}$) Dy^{3+} doped LCP samples were found to be between 5.19 and 5.52 eV utilizing the DRS investigation. Using the PL spectra, samples show yellow emission at 573 nm ($^4F_{9/2}\rightarrow {}^6H_{13/2}$) when excited at 347 nm ($^6H_{15/2}\rightarrow {}^6P_{7/2}$),andconcentration quenching, lifetimeanalysis, CCT, CP and photoluminescence quantum yield (02%). The material's strong yellow emission is confirmed by photometric studies and PL analysis. As by concluding results, the samples can be suitablefor yellowish light emitting solid state lighting devices.

1. Introduction

Nanomaterials are significantly more interesting than bulk materials because of their optical, electrical and magnetic characteristics. In the recent decade, researchers have focused a lot of their scientific attention on nanostructured materials because of their exceptional quantum confinement capabilities and maximum surface to volume ratio. Luminescence occurs when phosphors are subjected to UV light, X-rays, or other excitations.[1–3] The exceptional optical characteristics of rare-earth (RE) ion doped phosphors, such as their high quantum efficiency, adjustable emission color, and superior thermal stability, have made them a mainstay among the many kinds of luminous materials.[4]These features make them widely used in photovoltaic systems, flat panels and light-emitting diodes. Heat reflectors, smart windows, solar panels, display devices, and sensors are just a few of the many applications.[5,6]

Phosphors are utilized in fabrication of solid-state lasers, light converters, optical amplifiers, and optical thermometers, among optoelectronic devices. White light emitting diodes are essential to many industries, including display technology, medical illumination, outdoor lighting, etc.[7,8]Additionally, selecting suitable host material is crucial for versatile performance phosphor production.The crystal structure and characteristics of the host material have a significant impact on luminescence and phosphor efficiency. Thus, significant thought and host material optimization are required to prepare phosphor with the appropriate performance characteristics.[7,9]The phosphors with A = Li, K, and Na and B = Sr, Ca, and Ba cations are examples of $ABPO_4$structure that have been thought to be promising and have intriguing properties in light-emitting diodes (LEDs).[10]By adding RE elements to semiconductor photocatalysts, luminescence and environmental remediation may be enhanced.[11]RE elements like $Pr^{3+,}$ Dy^{3+}, Eu^{3+}, $Tb^{3+}$and Sm^{3+} are examples of activators. RE ions are extremely sought after for various applications, *via*.. lighting and display technologies, because of their emission capabilities and vibrant hues, which are particularly noticeable in the visible light spectrum.[12–14]Infrared and visible light are among the wavelengths at which RE ions can display photoluminescence due to their extraordinarily varied electronic structure.[15]Applications in optoelectronics, displays, and lighting are expanded by the improvement of luminous centers made possible by the addition of RE ions to the host's lattice structures. Different REemits in different locations based on their energy levels, and the color output can be altered to fit certain requirements and applications.[16]Many different kinds of materials show self-activated host emissions. They don't need to be doped with activator ions, which are usually lanthanides like Pr, Sm, Dy, Eu, and Tb. If a certain lanthanide or any activator ion is doped in such a host, the host can effectively transfer the excitation energy to the higher energy level.[17,18]The current study intends to prepare Dy^{3+} doped LCP NPs using a SSR technique.There are no available reports oncharacteristics of LCP doped with rare earth ions.Thestructural, morphological, vibrational, optical, and luminescent properties of the prepared sampleswere investigated to understand itsapplicability insolid state lighting devices.

2. Materials and Methods

The SSR approach was used to prepare pure and Dy^{3+} doped LCP NPs in different concentrations of 0.01, 0.05, and 0.09 mol%. All the precursors used in the preparation are ofAR-grade, ammonium dihydrogen orthophosphate (99.9% $NH_4H_2PO_4$), lithium carbonate (99.9% Li_2CO_3), cadmium oxide (99.9% CdO), and dysprosium oxide (99.9% Dy_2O_3), were used to prepare thepure and Dy^{3+} doped LCP NPs samples.The necessary precursors were first weighed in stoichiometric ratios according to their molecular weights and were ground until wellmixed powderusing a pestle andagate mortar.[2,9]

Then the grounded samples were sinteredat 500°Cfor two hours in a controlled muffle furnace. The sample was taken out from the furnace and was allowed to cool to room temperature later it wasgrounded once again for two hours.Again, the sample was sintered at 980°C for two hours. Then samples were taken out and were let to cool to room temperature. Finaly the sample was grounded for two hours and to get very fine powder. Figure 1 illustrates the methods for synthesizingpure and Dy^{3+} doped LCP NPs.[19,20]

3. Instrumentation

For structural analysis, the P-XRD pattern was recorded from 10° to 90°of 2θusing the Malvern Panalytical Ltd., Empyrean model Powder X-Ray diffractometer at stepwise scanning rate of 0.02° and time per step at 0.4 s. The wavelength of the copper (K_α) radiation employed was 1.5418 Å. The elemental analysis was conducted using INCAx-act OXFORD EDS, whereas the surface morphological study was carried outusing Ultra 55 ZeISS FE-SEM. SHIMADZU IRAffinity-1S FT-IR Spectrophotometer was used to record the vibrational bands with a wavelength range of 400 to 4000 cm^{-1}. Raman spectra were recorded by Renishaw in Via Micro Raman Spectrometer at a resolution of 3 cm^{-1} by using a laser that excites materials at a wavelength of 532 nm. DRS spectra recorded using UV-Vis-NIR Spectrometer (JASCO UV V-770 model). Edinburgh Instruments FLS 980 spectrofluorometer has been used for photoluminescence studies.

4. Results and discussions

4.1 Powder XRD scrutiny

An X-ray beam is projected onto a sample using the Powder X-ray diffraction (P-XRD) technique, which then calculates the intensity and angle of the diffracted X-rays. The resulting P-XRD pattern was used to determine the sample's phase and crystal structure.[6,9] The resulting P-XRD pattern showed clear, broad and prominent peaks. According to the sharp peak intensities shown by XRD, the synthesized material was incredibly pure and crystalline. The major and minor peaks on the LCP and JCPDS Card no.01-081-0508 data have identical positions and intensities. TheP-XRD pattern ofstandard PDF file. Pure and Dy^{3+} doped LCP NPs are shown in Fig. 2. Table 1 lists the pertinent lattice parameters that are determined using unit cell software.[21]Using Debye Scherrer's formula and W-H plot method, the average crystallite size was determined. Additionally, micro strain(ε)anddislocation density (δ)values are determined using the Stokes-Wilson (S-W's) and Williamson-Smallman (W-S's) relations. Table 2 displays the computed **s**tructural parameters like crystallinity size, micro strain, dislocation density, crystallinity index, lattice structure of the prepared samples.[22,23]**Figure3**shows the plottedW-H plots.

Dy^{3+} ions should occupy any of Li^+ or Cd^{2+} ion locations in the crystal lattice. For the Li^+ ion(0.76 Å, CN = 6), the Cd^{2+} ion (0.95 Å, CN = 6), and the Dy^{3+} ion (0.91 Å, CN = 6). In the host lattice LCP NPs, Dy^{3+} is likely to replace Cd^{2+} due to their closer match in coordination numbers and ionic radii,and also the lattice charge can be balanced by a large concentration of Cd vacancies and comparable coordination numbers and ionic radii.[24]

Table 1

Pure and Dy^{3+} ions doped LCP NPs lattice parameters

Parameters		**JCPDS:01-081-0508**	**Pure**	**$Dy_{0.01}$**	**$Dy_{0.05}$**	**$Dy_{0.09}$**
Crystal Structure		Orthorhombic	Orthorhombic	Orthorhombic	Orthorhombic	Orthorhombic
Space Group		Pnma	Pnma	Pnma	Pnma	Pnma
Lattice Parameters	a (Å)	10.7240	11.0565	11.0018	11.0297	11.0294
	b (Å)	6.2880	6.2334	6.2529	6.2758	6.2761
	c (Å)	4.8040	4.7750	4.7736	4.7740	4.7750
	α°	90.0000	90.0000	90.0000	90.0000	90.0000
	β°	90.0000	90.0000	90.0000	90.0000	90.0000
	γ°	90.0000	90.0000	90.0000	90.0000	90.0000
Volume ($Å^3$)		323.95	329.10	328.39	330.45	330.54

Table 2

Structural parameters crystallinity size, micro strain, dislocation density, crystallinity index, lattice structure and phase space group of synthesized samples

Sample	Debye Scherrer's method			W-H plot method			Crystallinity index (%)	Lattice Structure	Phase space group
	Crystallite size (D nm)	**Micro strain (ε)**	**Dislocation density (δ) (lines/m^2)**	**Crystallite size (D nm)**	**Micro strain (ε)**	**Dislocation density (δ) (lines/m^2)**			
Pure	31.49	25.4×10^{-4}	1.007×10^{15}	32.17	82.33×10^{-4}	0.966×10^{15}	96.90	Orthorhombic	Pnma
$Dy_{0.01}$	37.03	30.50×10^{-4}	0.730×10^{15}	31.80	42.47×10^{-4}	0.988×10^{15}	94.38		
$Dy_{0.05}$	35.67	41.10×10^{-4}	0.786×10^{15}	31.15	31.40×10^{-4}	1.030×10^{15}	92.48		
$Dy_{0.09}$	34.20	31.70×10^{-4}	0.855×10^{15}	30.88	13.30×10^{-4}	1.049×10^{15}	91.71		

4.2 Morphology studies and EDS analysis

An essential technique for characterizing a sample is FE-SEM analysis, which yields details about its topography, shape, grain size, and growth mechanism. Figure 4represents the FE-SEM images of prepared LCP NPs. The morphology of the prepared samplesdisplaysclustered irregular stone-like structure. The average particle size of prepared sampleswascalculated, as evaluated by a FE-SEM picture at a magnification of 200 nm, and isshown in Fig. 5. The average grain size, which is 52.19 nm, 76.13 nm, 70.93 nm and 77.26 nm for pure and Dy^{3+} doped LCP NPs, was determined by collecting 50 identical particles using ImageJ software.Since a single particle may include many crystallites, the average particle size determined from FE-SEM images and the CS determined using Scherrer's techniques may not be similar. As a result, the average particle size ought to consistently exceed the crystallites.[25]

The EDS spectra show the composition ofelements present in the prepared samples such as Dy, Cd, P, and O,which was shown in Fig. 6. However, the typical EDS pattern is unable to identify lithium (Li) atoms because of significant absorption by the

surrounding heavier elements and surface layers.[26]

4.3 FT-IR analysis

Often, molecules with structural similarities were used to designate the several entities that comprise phosphate ions. Figure 7 displays the FT-IR spectra of Dy^{3+} doped LCP NPs in the 4000 – 400 cm^{-1}wave number range. The spectrum shows the several functional groups present in the stretching and bending vibrations of the sample. The vibrational band allocations of Dy^{3+} doped LCP NPs are listed in Table 3.[27,28]

Table 3
Band assignments for vibration in synthesized LCPNPs samples

IR Band position (cm^{-1})				**Vibrational mode**
Pure	**$Dy_{0.01}$**	**$Dy_{0.05}$**	**$Dy_{0.09}$**	
471	473	475	478	Symmetric bending mode of PO_4^{3-} ions
622	627	626	626	Asymmetric bending approach of the PO_4^{3-} ions
952, 1045, 1248	953,1044, 1140	957,1044, 1144	954, 1049	Asymmetric mode stretching bands of the PO_4^{3-} ions
1372	-	1359	-	P-O stretching
1747	1742	1744	1734	O-H bending vibration
2350	2352	2355	2356	Stretching vibration of P = O bond

4.4 Raman analysis

An established analytical technique for identifying the fully describing vibrational molecules and assessing the composite influence on materials is Raman spectroscopy.[29]The symmetric and asymmetric bands of PO_4 were identified in the 200–1300 cm^{-1} range, and their Raman data assignments are comparable to the FTIR spectrum shown in Fig. 7, where the υ_s (PO_4) band assignment is indicated by the prominent peak at the 957cm^{-1}regions.[30]**Table 4** shows the pure and Dy^{3+} doped LCP NPs Raman mode assignments which are illustrated in Fig. 8.

Table 4
Raman band assignments of synthesized LCPNPs samples

Wavenumber (cm^{-1})				**Assignments**
Pure	**$Dy_{0.01}$**	**$Dy_{0.05}$**	**$Dy_{0.09}$**	
216	229	225	226	External modes
444	437	439	452	δ_s (PO_4)
609	603	600	604	δ_{as} (PO_4)
929,957	926,959	929,961	927,957	υ_s (PO_4)
1010,1076	1009,1077	1010,1067	1012,1066	υ_{as} (PO_4)
1320	1359	1398	1332,1462	External modes

4.5 DRS analysis

Diffuse Reflection Spectroscopy (DRS) is an essential technique for examining the optical properties of nanostructured crystalline materials in the UV to NIR spectral range.Both pure and Dy^{3+} doped LCP's DRS spectra were captured in the 200–800 nm wavelength range.The visible band (350–500 nm) has a peak at 440 nm, whereas the UV zone (250–350 nm) has strong peaks at 204 nm, 259 nm, and 328 nm. Figure 9shows the DRS spectra of the obtained Dy^{3+} doped and pure LCP samples. Both the pure and Dy^{3+} doped LCP spectra have many peaks in the UV band, with wavelengths ranging from 200 to 400 nm.[31]The optical energy band gap of the prepared sample was also determined by plotting F(R) against energy using the Kubelka-Munk (K-M) method.

The function result, F(R) = 0, indicates that the optical bandgap values for the pure and $Dy_{0.01}$, $Dy_{0.05}$,$Dy_{0.09}$are 5.43 eV, 5.19 eV, 5.27 eV, and 5.52 eV, respectively. Figure 10 displays the optical direct energy bandgap graph of Dy^{3+} doped LCP NPs using the K-M function. which were covered in Table 5. Due to its wide bandgap, this material may be suitable for optical devices.[32,33]

Table 5
Energy band gap of synthesized LCP NPs

S.No	Sample	Bandgaps (eV)
1	Pure	5.43
2	$Dy_{0.01}$	5.19
3	$Dy_{0.05}$	5.27
4	$Dy_{0.09}$	5.52

4.6 Photoluminescence

At the emission wavelength of 573 nm, the excitation spectrum exhibits many peaks in the 275–500 nm range due to the 4f-4f electronic transitions of Dy^{3+} ions.Excitation peaks in the spectra, such as297, 323, 347, 362, 383, 424, 452 and 473 nm with the transitions $^6H_{15/2}$→ $^6D_{7/2}$,$^6P_{3/2}$, $^6P_{7/2}$, $^6P_{5/2}$, $^4I_{13/2}$,$^4G_{11/2}$,$^4I_{15/2}$and $^4F_{9/2}$.[34,35]The Dy^{3+} doped LCP NPs' excitation spectra are shown in Fig. 11.

At the highest excitation wavelength (λ_{ex} = 347 nm), the emission spectra of Dy^{3+} doped LCP NPs are displayed in Fig. 12.The electronic transitions from $^4F_{9/2} \rightarrow {}^6H_{15/2}$, $^6H_{13/2}$, $^6H_{11/2}$, and $^6H_{9/2}$ of Dy^{3+} ions are responsible for the emission peaks seen in the spectra at wavelengths of 482 nm, 573 nm, 661 nm, and 756 nm.[36–38]The schematic energy level diagram was shownon**Figure 13.**

The lifetime decay curves of prepared LCP NPs samples were shown in Fig. 14. The fitting of each prepared sample's decay curves with a double-exponential functionfor getting better representationin the graph. The lifetime decays of Dy^{3+} doped LCP NPs calculated with (Eq. 1)**Eq. 1**are displayed in Table 6.[39]

$$\tau = \frac{A_1 \tau_1^{\,2} + A_2 \tau_2^{\,2}}{A_1 \tau_1 + A_2 \tau_2} \rightarrow (1)$$

Table 6
Lifetime decays of of Dy^{3+} doped LCP NPs

Samples	$\varvec{\tau_{avg}}$(ms)
$Dy_{0.01}$	0.50
$Dy_{0.05}$	0.42
$Dy_{0.09}$	0.39

Emission spectra indicates that concentration quenching occurs when the amount of Dy^{3+} in the host matrix increases by 0.05%. The emission intensity falls as the concentration of Dy^{3+} ions rises because the distance between nearby Dy^{3+} ions shrinks and the Dy cross-relaxation mechanism is triggered.A weak or mixed multipolar interaction might cause cross-relaxation. The magnitude of the critical distance (R_c) can be utilized to determine the kind of interaction mechanism of Dy interacting in Dy^{3+} doped LCP. Exchange interactions take place when R_c is less than 5 Å, whereas multipolar interactions happen when R_c is greater than 5 Å.[40]The Blasse equation can be used to determine the value of R_c, which is represented by **Eq. 2.**[41,42]

$$\mathrm{R_c} = 2\left(\frac{3V}{4\pi\ \mathrm{ZX_c}}\right)^{1/3} \rightarrow (2)$$

where V (= 330.45 $Å^3$) is the unit cell's volume, Z is the number of accessible cationic sites, and X_c(0.05%) is the ideal concentration of Dy^{3+} ions in the host matrix.The multipolar contact between Dy^{3+}-Dy^{3+} is responsible for energy transfer since the computed value of R_c is 74.93 Å, which is higher than 5 Å.According to Dexter's theory, concentration quenching results from multi-polar interaction. To identify the kind of multipolar interaction, utilize **Eq. 3**:

$$\frac{I}{\mathrm{X}} = \mathrm{k}\left[1 + \beta\,(\mathrm{X})^{Q/3}\right]^{-1} \rightarrow (3)$$

where Q is the type of multipolar interaction, I is the integrated intensity, X is the concentration of Dy^{3+} that is equal to or higher than the ideal concentration, and k and β are constants.The Q value obtained indicates that the interaction is weak or mixed multipolar, in accordance with Dexter's theory. When considering β[(X)]^(Q/3)≫1, **Eq. 3** minimized to

$$\log\left(\frac{I}{\mathrm{X}}\right) = C - \frac{Q log\,(X)}{3}\ :$$

here C = log k-log β

The log(I/x) vs. log(x) plot is shown in Fig. 15. R^2 = 0.780 shows that the experimental data are linearly fitted, and the fitted data's slope (-Q/3) is -1.14.Q's determined value is 3.42, which is closer to 6. Intensity drops at 0.05% verify the concentration quenching.[41,43]

To determine the phosphor material's photoluminescence efficiency, one crucial metric is the photoluminescence quantum yield (PLQY).The ratio of photons released to all photons absorbed under specific excitation circumstances is known as the quantum yield in mathematics.[44]An integrating sphere within the FLS980 spectrometer was used to measure the PLQY.The 120mm PTFE integrating sphere has a reflectance of approximately 95% in the 250–2500 nm spectral area and 99% in the 400–1500 nm range. A sample in the integrating sphere and incident beam path was employed for direct measurement. A reflective PTFE standard, such as the integrating sphere, is loaded in the absence of a sample.The baffle prevents the sphere from being immediately excited by light from the excited source via the emission port.[45,46]A sample is positioned in the integrating sphere in the incident light path, and a reflecting standard is placed in an empty sphere as part of the measuring procedure. Eq. (4) determines the PLQY value of 2% which was represented in Fig. 16.Due to non-radiative relaxation caused by high-energy

phonons, cross-relaxation, concentration quenching, and yellow light emission in Dy^{3+} ions as an outcome of parity-forbidden4f-4f transitions with low absorption cross-sections, currently used phosphors' quantum yield is low.[47,48]

$$\mathrm{PLQY} = \frac{\mathrm{Em_2} - \mathrm{Em_1}}{\mathrm{Ex_1} - \mathrm{Ex_2}} \% \rightarrow (4)$$

where Ex_1, Ex_2, and Em_1, Em_2 stand for the number of photons found in the emission wavelength region for the empty sphere measurement and a sample in the sphere placed in the light beam's path, respectively, and the number of photons found in the excitation wavelength region for the empty sphere measurement and a sample in the sphere placed in the light beam's path.

for λ_{ex} = 347 nm

4.7 Photometric analysis

The Dy^{3+} doped LCP NPs CIE chromaticity diagram was shown on**Figure 17**. The prepared sample's photometric characteristics, such as CIE coordinates, color purity andCCTwere measured using CIE OSRAM software and are displayed in Table 7. The yellowish zone was found to contain the CIE color coordinates (x,y) = (0.4642, 0.4875), (0.4686, 0.4910) and (0.4642, 0.4873) of 0.01%, 0.05%, and 0.09% of Dy^{3+} doped LCP, respectively.[3]

Table 7

Photometric parameters of Dy^{3+} doped LCP NPs

Compound	CIE Color coordinates (x,y)	Color purity (%)	CCT(K)
$Dy_{0.01}$	(0.4642, 0.4875)	85.8	3173
$Dy_{0.05}$	(0.4686, 0.4910)	88.1	3135
$Dy_{0.09}$	(0.4642, 0.4873)	85.7	3171

An essential photometric metric for assessing emission spectrum data of synthesized samples.Table 7 displays the statistical importance of each photometric parameter.These parametric discoveries could be useful for the synthetic materials used in LEDs and other photo-responsive devices that create warm light.High-density optical units and color display systems can also employ them.[35,49]The synthesized materials may find application in optical devices like yellow lighting applications, according to these parametric results.

5. Conclusion

Pure and Dy^{3+}doped $Li_2Cd_2(PO_4)_2$ samples were synthesized by a solid-state reaction (SSR) method. Using P-XRD data, the crystallite sizes of the sampleswere obtained by using Debye-Scherrer formula and Williamson-Hall (W-H) plot techniqueand were estimated to vary between 31 and 37 nm.Clustered and irregular stone-likesurface morphology of the samples was observed by the FE-SEM, and average particle sizes were also determined.EDS analysis was carried out to identify the elements present in the sample.Bandgapsfor the pure and Dy^{3+}doped LCP sampleswere estimated by DRSanalysisand are 5.43 eV (pure), 5.19 eV, 5.27 eV and 5.52 eV, respectively.PO_4^{3-} vibrational bands were determined byFTIR and Raman spectroscopies. PL spectrum of the Dy^{3+}doped LCP samples excited with 392 nm showed prominent emission band located at 573 nm ($^4F_{9/2} \rightarrow {}^6H_{13/2}$).Additionally,lifetime decay analysis, concentration quenching and photoluminescence quantum yield (PLQY) measurement were determined using PL data. Color Purity (CP) and Correlated Color Temperature (CCT) werealsoanalyzed. From the above analysis, the prepared samples are suitable for yellowish light-emitting solid-state lighting devices.

Declarations

Competing interest and declaration

The authors state that none of the research described in this analysis appears to have been impacted by any known financial conflicts of interest or intimate personal ties.

Funding statement

No financial support is provided for any kind of research and analysis work.

Statement of Data Availability

Data will be provided by the author upon request.

ORCID ID's

Shaik Azad Bashahttps://orcid.org/0000-0001-8132-8486

K. Srinivasarao https://orcid.org/0000-0002-9970-6243

K. Daniel https://orcid.org/0009-0003-8525-122X

B.V Naveen Kumar https://orcid.org/0000-0003-4700-5442

Y. Nirmal Rajeevhttps://orcid.org/0000-0002-5982-8983

Prof. Sandhya Cole https://orcid.org/0000-0002-1827-2149

Author Contribution

Shaik Azad Basha: Data curation, Methodology, Resources, Writing- original draft. K. Srinivasarao: Visualization, Software, Methodology. K. Daniel:Conceptualization, Data analysis, Validation. B. V. Naveen Kumar: Resources, Software, Validation. Y. Nirmal Rajeev:Methodology, Resources,Data analysis.Sandhya Cole: Conceptualization, Validation, Writing-review & editing.

References

1. Shrivastava R, Kaur J, Dubey V (2016) J Fluoresc 26:105
2. Basha SA, Cole S (2024) D. Divakaran andI.Suyambulingam, Springer Proc. Mater.,60, 667
3. Tejas A, Princy S, Kennedy MM, Rashad M, Sayyed MI, Kamath D (2024) J Lumin 275:120741
4. Hussain SK, andJ WX (2025) S.Yu, Ceram. Int., 51, 41354
5. Muswareen SK, Rao MS, Sridevi G (2019) andS Cole Mater Sci Semicond Process 102:104588
6. Kumar JS, Lakshmi NR, Neeraja K, Devi TA, Swamy DT, Basha SA (2025) S Cole Asian J Chem 37:1204
7. Poria K, Lohan R, Kumar SBA, Singh R, Deopa N, Punia R, Shahi JS (2023) and A. S.Rao, RSC Adv.,13, 11557
8. C.Jayachandraiah K, andN (2015) J Madhusudhana Rao Alloys Compd 623:248
9. Rao KS, N.Kumar BV, N.Rajeev Y, andS KV, Cole (2023) J Mol Struct 1284:135406
10. Dash (2022) Pradhan andS. J Rare Earths 40:1837
11. Kaur P, Khanna A, Singh MN, andA K, Sinha (2020) J Alloys Compd 834:154804
12. Xu M, Yang X, Yang XA, Zhou L, Liu TZ (2010) Z Fan andT Jiang Prog Chem 22:861
13. Djamal M, Yuliantini L, Hidayat R, Boonin K (2018) P.Yasaka and J.Kaewkhao, Mater. Today Proc.,5, 15126
14. Balasubramanyam SV, Srinivasarao K, Basha SA (2025) S Cole Res Methodol Mat Sci 29:145
15. Gupta SK, Ghosh PS, andV AA (2014) Natarajan RSC Adv 4:51244
16. Basha SA, Naveen Kumar BV, Daniel KSK (2026) S V Balasubramanyamand S Cole Phys Chem Res 14:173
17. Guo H, Shi Q, Ivanovskikh KV, Wang L (2020) C.Cui and P.Huang. Mater Res Bull 126:10836

18. V.Kumar S, Duvenhage OM (2014) H C Swart Appl Surf Sci 308:419
19. Daniel K, Kumar BVN, Rajeev YN (2024) K Venkatarao S Cole Phys E Low Dimens Syst Nanostruct 159:115911
20. Rao KS, Venkatarao K (2023) Rajeev andS. Cole Phys Chem Res 11:501
21. Li XZ (2005) Ultramicroscopy 102:269
22. D.Divakaran M, Sriariyanun SA, Basha I (2023) Sanjay andS Siengchin Biomass Convers Biorefin 14:23825
23. Rani GR, Kuna S, Kodamala D (2025) Basha andS. Cole Next Mater 8:100819
24. J.Gao R, Yang X, Yong MS, Zhao Y (2023) J Lumin 255:119583
25. Balasubramanyam SV, Rao KS, Daniel K, Basha SA (2025) S Cole Phys Chem Res 13:463
26. Anjaneyulu NC, K.Suresh YV, Vasu G, Ramana GV (2024) S. S. N.Ravikumar. Mater Res Innov 28:1
27. Frost RL, Scholz R (2014) A.López andY.Xi,Spectrochim. Acta Mol Biomol Spectrosc 124:243
28. S.Mukherjee DP, Tyagi K (2013) J Lumin 134:880
29. D.Janardhana SN, Jayaramu E, Motaung (2024) and H. C.Swart, Mater. Sci. Semicond. Process.,184, 108789
30. Lamsaf H, Fausto R, Costa BFO, Elghadraoui JTEH (2018) M Ijjaali Oulmekki Mater Chem Phys 216:22
31. Lee GH, Kim TH, andS CY, Kang (2008) J Lumin 128:1922
32. Munimasthani S, Sarathkumar S, andR UST, Ravikumar VSSN (2020) Appl Phys Mater Sci Process 126:1
33. Daniel K, Venkatarao K, Srinivasarao K, Basha SA, Cole S (2021) ANU J Phys Sci 13:53
34. Cao R, Zheng Y, Chen T, Lan B, Li L, Zhong Q, Nie S (2022) J Wang J Mol Struct 1262:133008
35. Raghupathi P (2022) andB. C.Jamalaiah. J Mol Struct 1268:133695
36. R K, P.A,M. M.Kennedy V, I.Sayyed MR (2025) S D Kamath Phys B Condens Matter 697:416712
37. Revannasiddappa GR, Basavaraj RB, Rudresha MS, Nagaraju G, Kumar S (2021) N Sasidhar 184:109940
38. Sheoran M, Kumari PSN, Malik SPKRK (2021) Chem Phys Lett 773:138608
39. Naveen Kumar BV, Venkata Rao K, Shaik EB, Rajeev YN, Rao KR (2022) S Cole Luminescence 37:1942
40. K.Satyavathi MS (2017) Rao,Y.Nagabhaskararao andS. Cole J Mater Sci: Mater Electron 28:12226
41. andA IK, Gathania K (2022) J Mater Sci: Mater Electron 33:328
42. Mebarki L, Kahouadji B, Zoukel A, D.Poelman and, C.Swart H (2024) J Fluoresc 35:5391
43. M. Fhoula andM.Dammak. J Lumin. 210, 1(2019)
44. P.Singh,H.Mishra and S. B.Rai, Sci Rep, 13, 1(2023)
45. N.Ogugua S, K.Shaat SK, Swart HC, Kroon RE, M.Ntwaeaborwa O (2019) J Alloys Compd 775:950
46. N.Kumar BV (2025) H. C. Swart andR. E.Kroon, Opt. Mater.,167, 117274
47. Beck AR, S.Das and, Manam J (2017) J Mater Sci: Mater Electron 22:17168
48. C.Mohan T, Dinesh PS, N.Devara BS (2025) T. R. Raman andY. C.Ratnakaram, Luminescence., 40, e70288
49. Saraswat Y, Bhardwaj C, Kumari S, Prasad A, andA (2024) S Rao J Mater Sci: Mater Electron 35:1

Figures

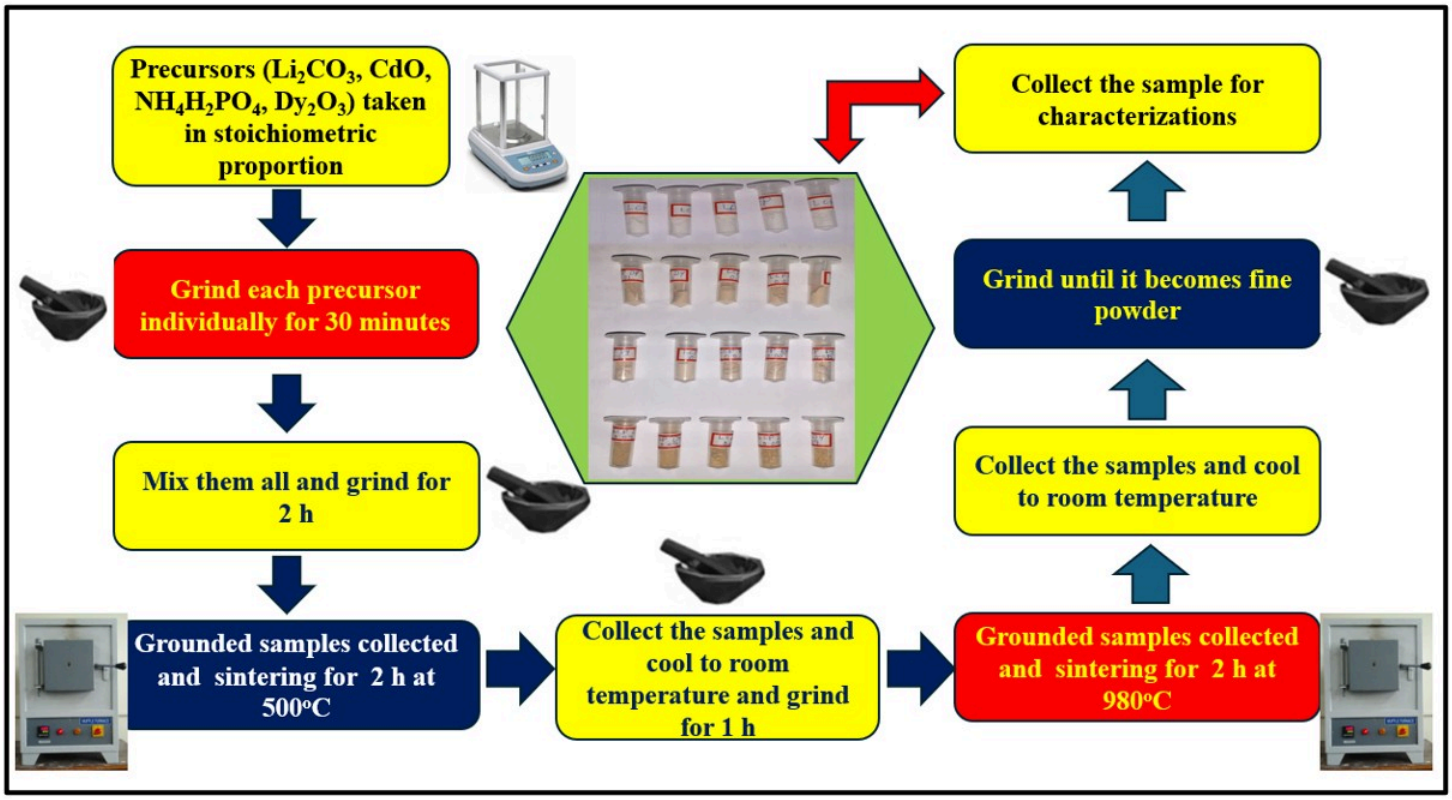


Figure 1

Schematic representation ofsamples preparation

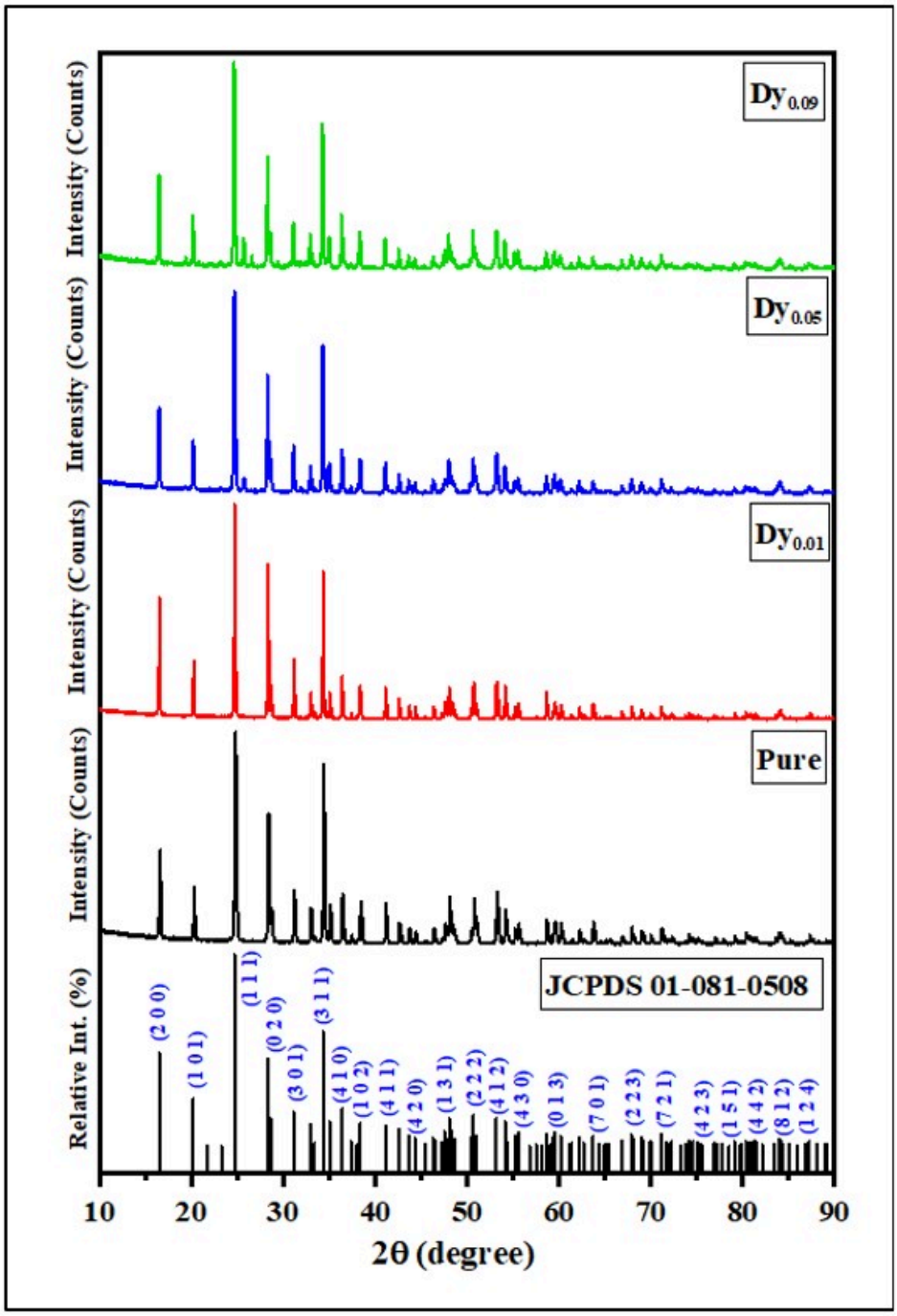


Figure 2

Comparative XRD patterns ofsynthesized samples with JCPDS data

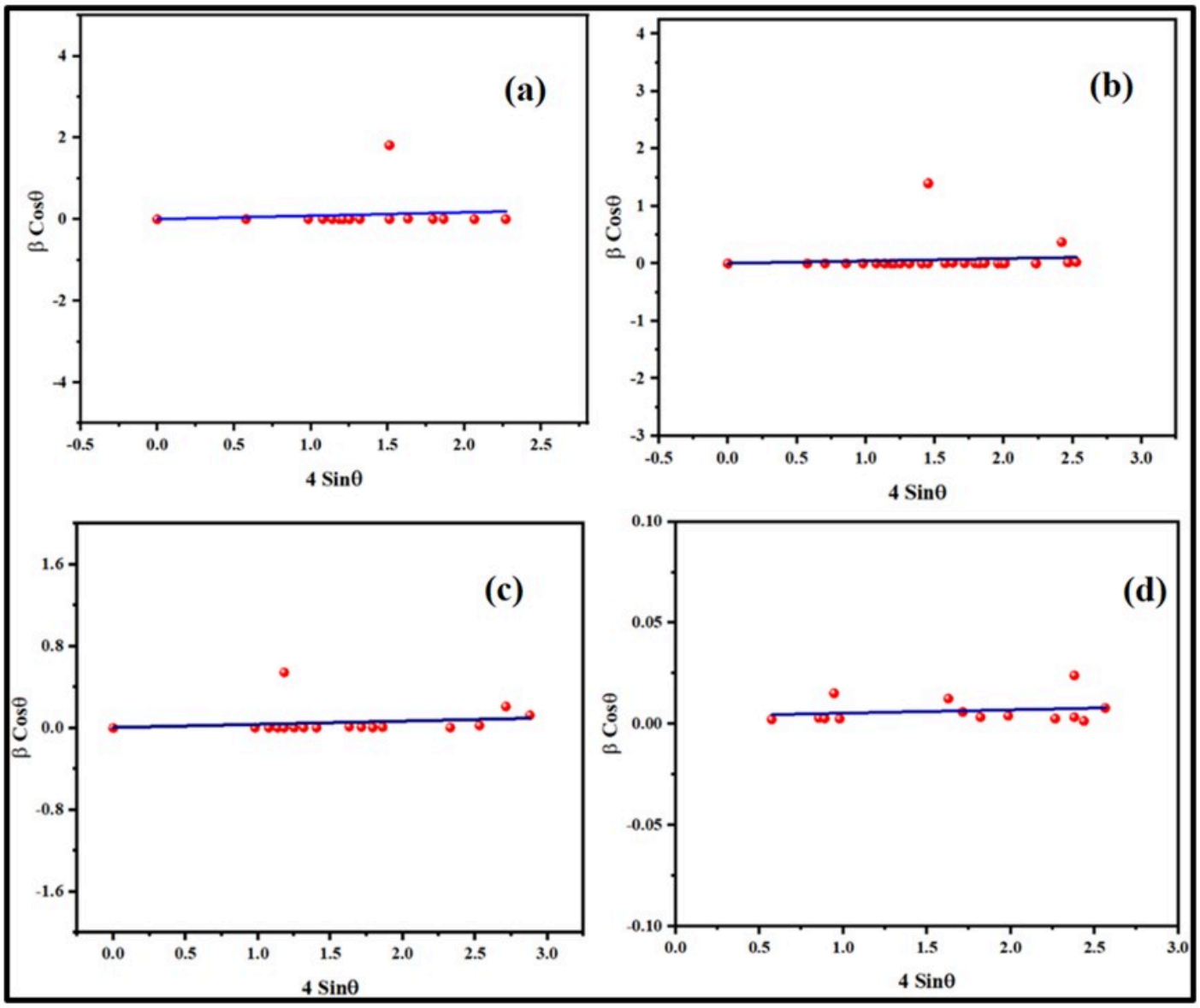


Figure 3

W-H plots of (a) Pure (b) $Dy_{0.01}$ (c) $Dy_{0.05}$and (d) $Dy_{0.09}$

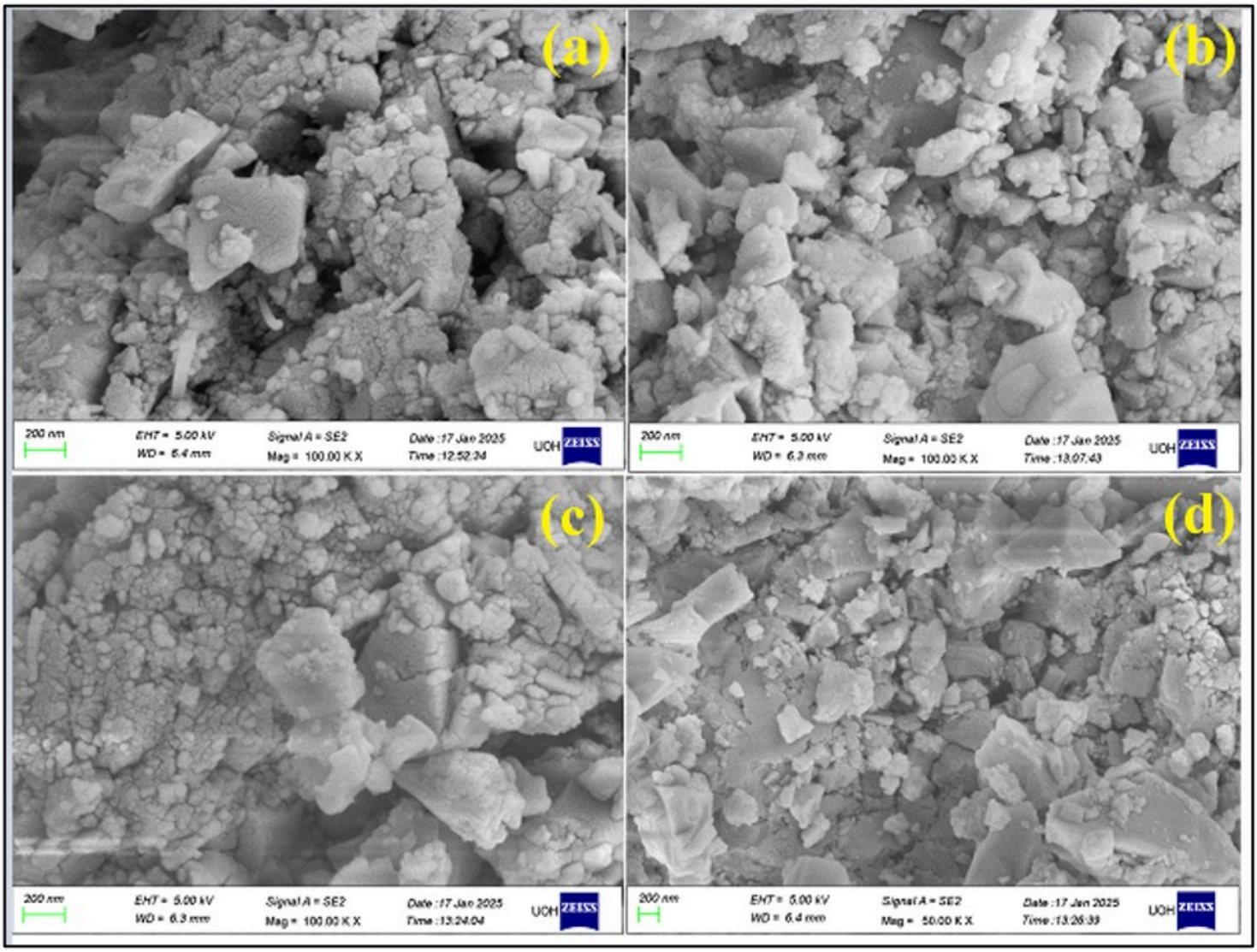


Figure 4

FE-SEM images of (a)Pure (b) $Dy_{0.01}$(c) $Dy_{0.05}$(d) $Dy_{0.09}$

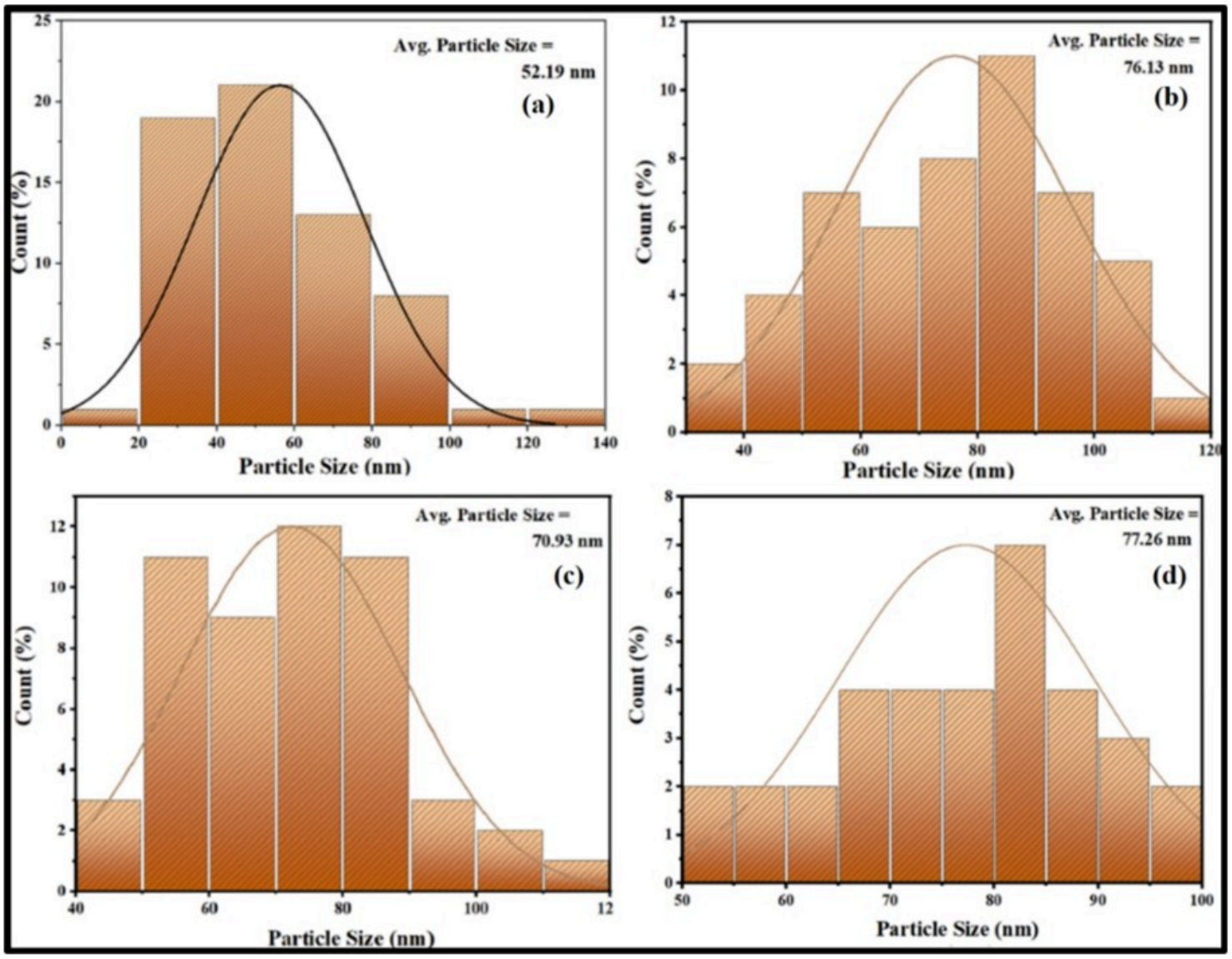


Figure 5

Histograms of Avg. particle sizeof (a) Pure (b) $Dy_{0.01}$ (c) $Dy_{0.05}$ (d) $Dy_{0.09}$

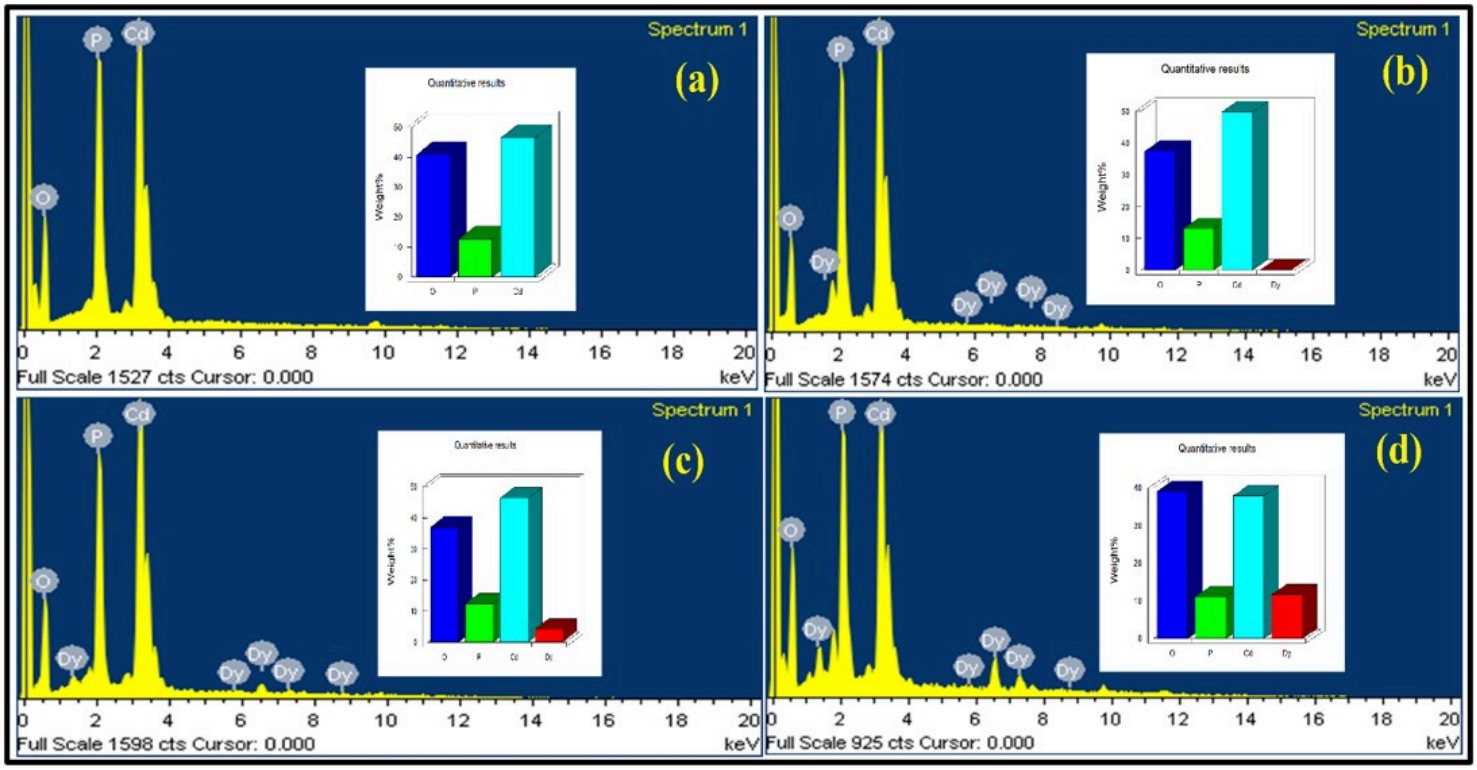


Figure 6

EDS elemental mapping of (a) Pure (b) $Dy_{0.01}$ (c) $Dy_{0.05}$and (d) $Dy_{0.09}$

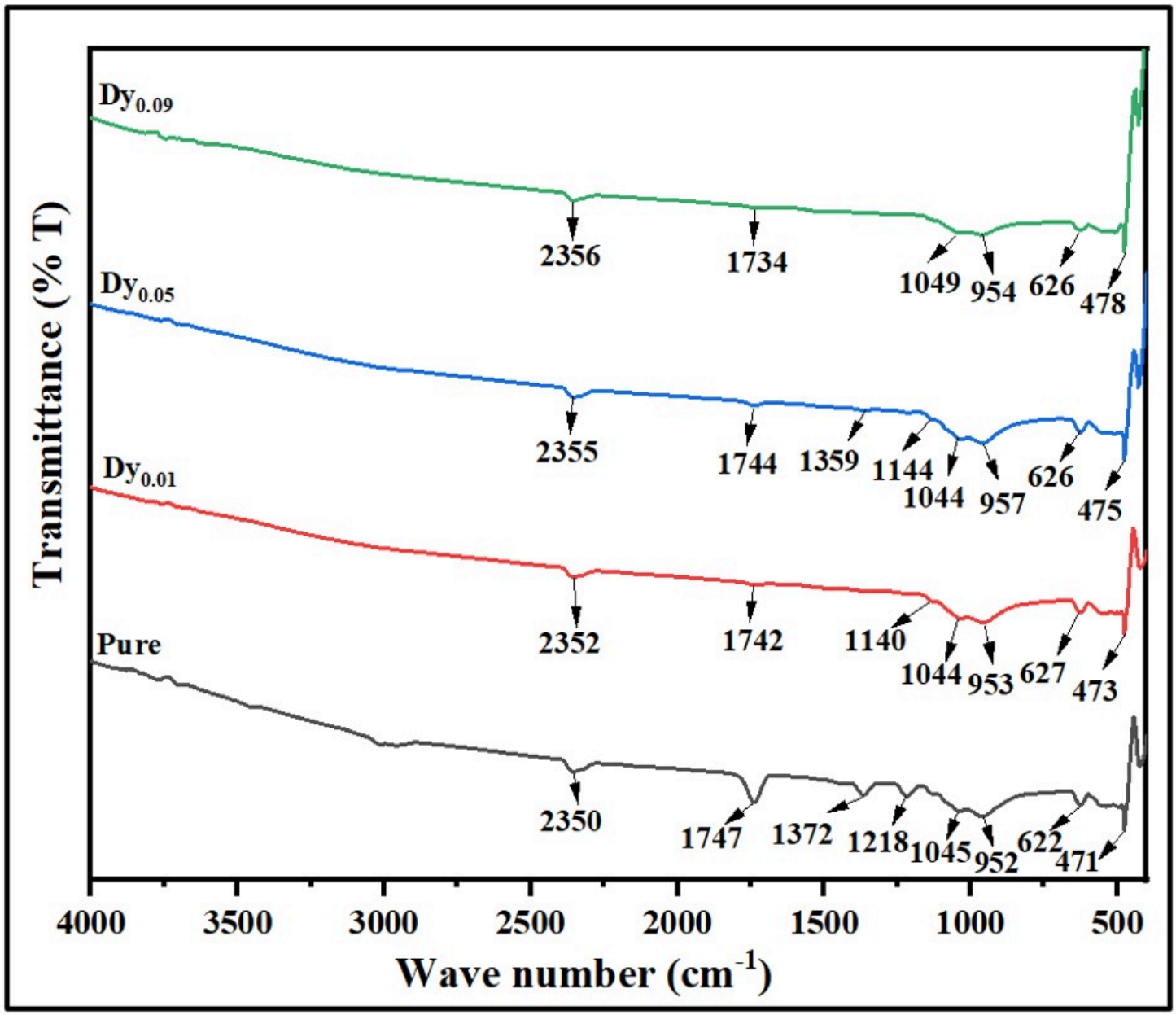


Figure 7

FT-IR spectrum of synthesized LCPNPs samples

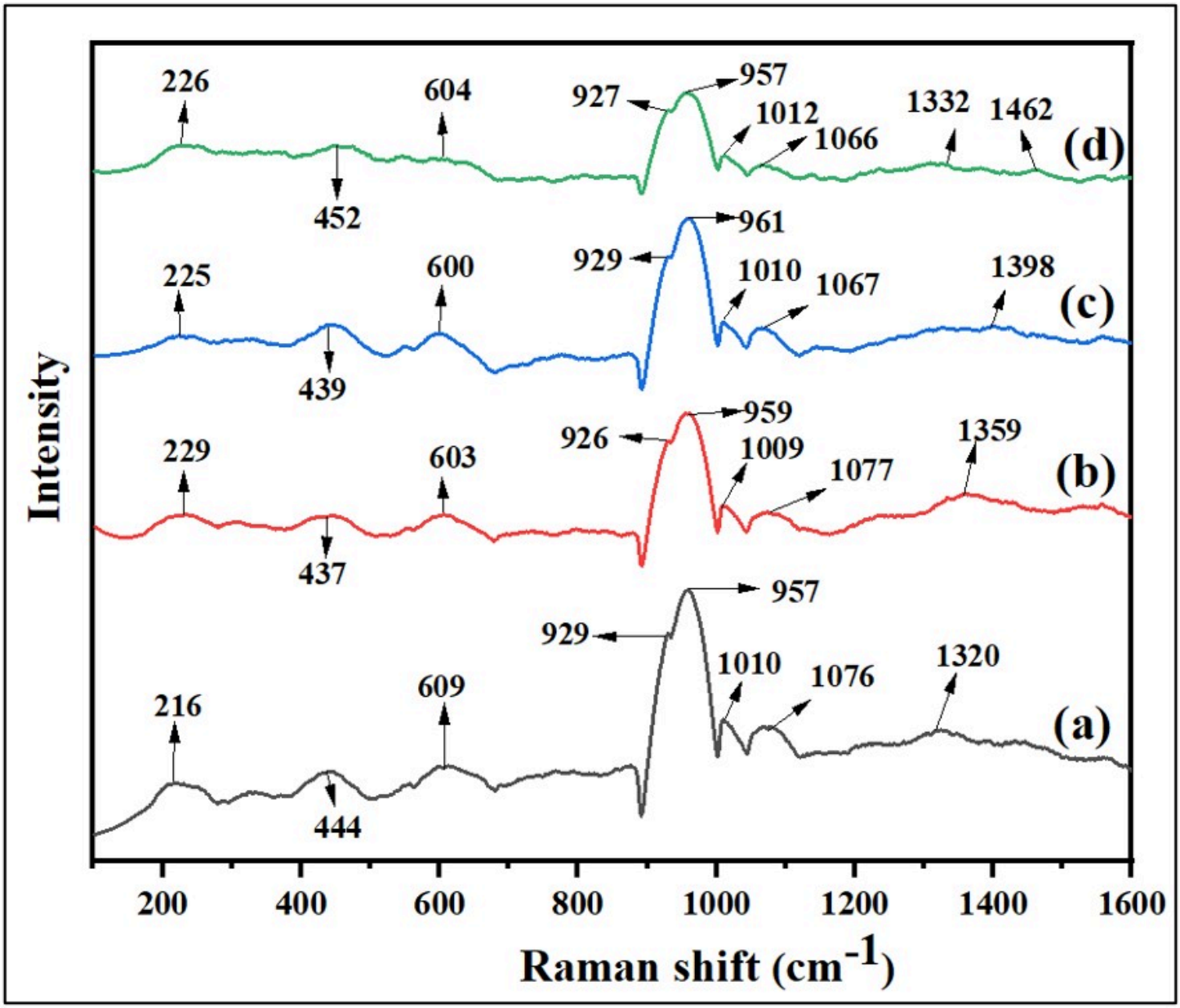


Figure 8

Raman spectra of (a) Pure (b) $Dy_{0.01}$ (c) $Dy_{0.05}$and (d) $Dy_{0.09}$

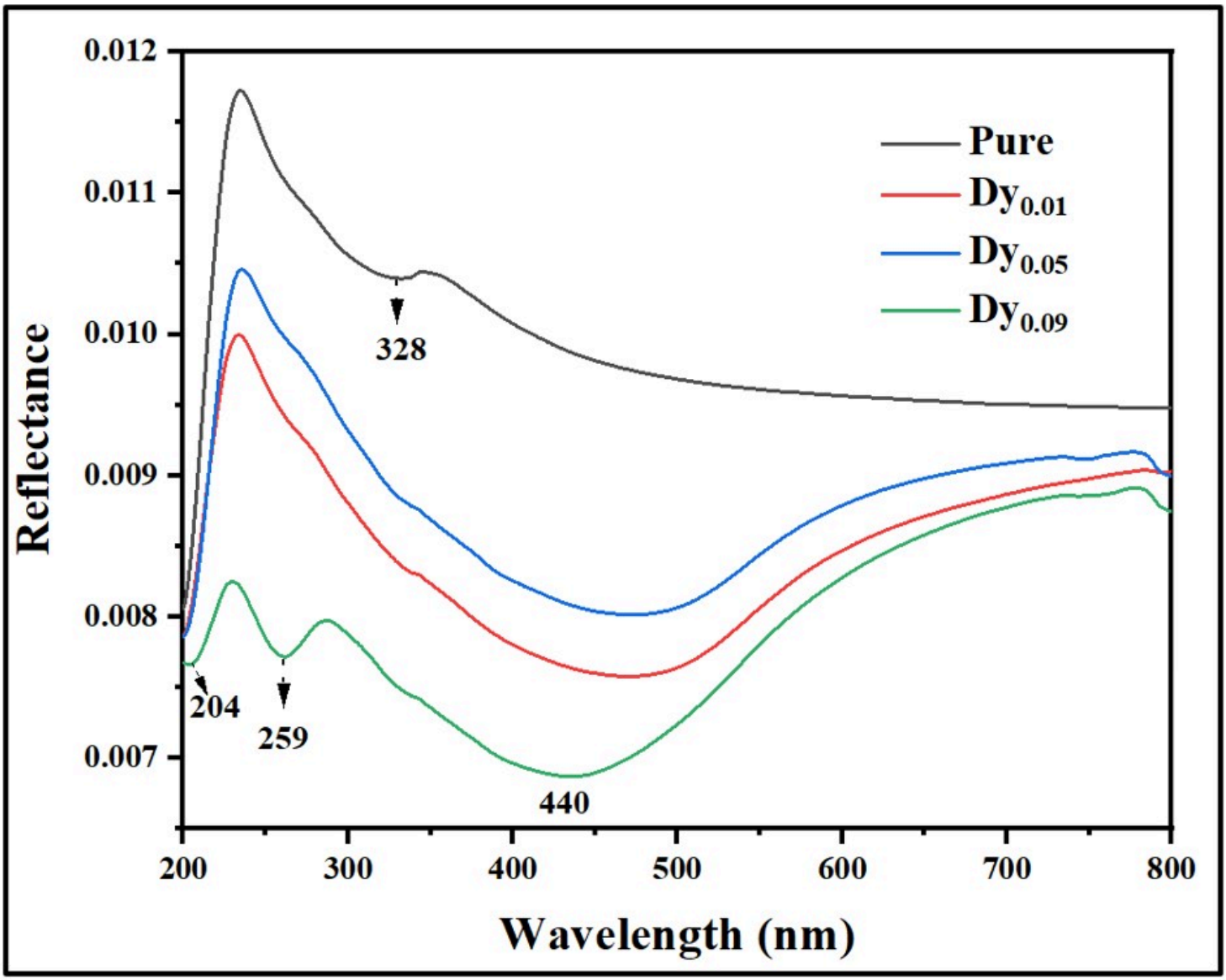


Figure 9

DRS spectra of synthesized LCPNPs samples

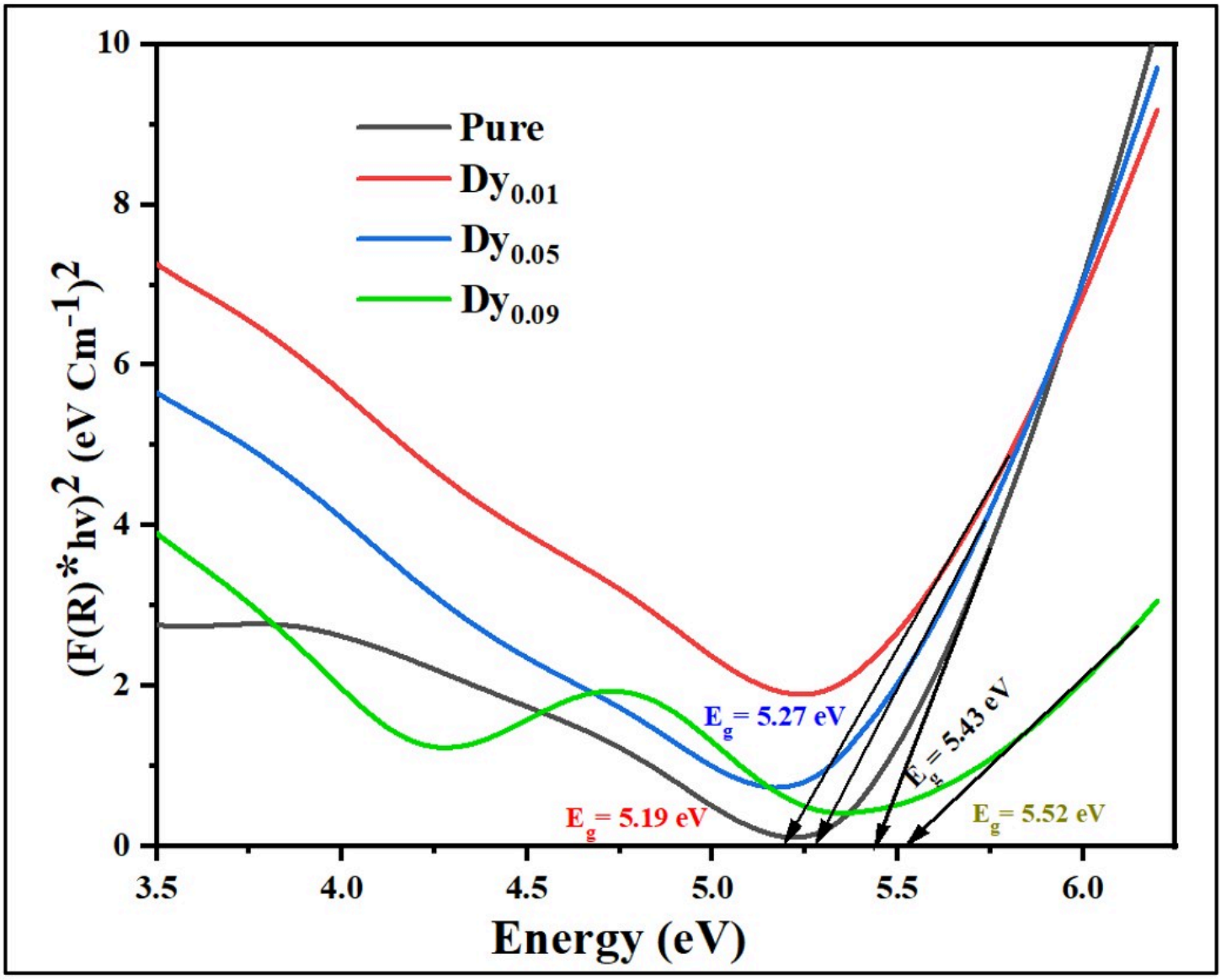


Figure 10

Optical energy band gap of LCP NPs doped with Dy^{3+} ions

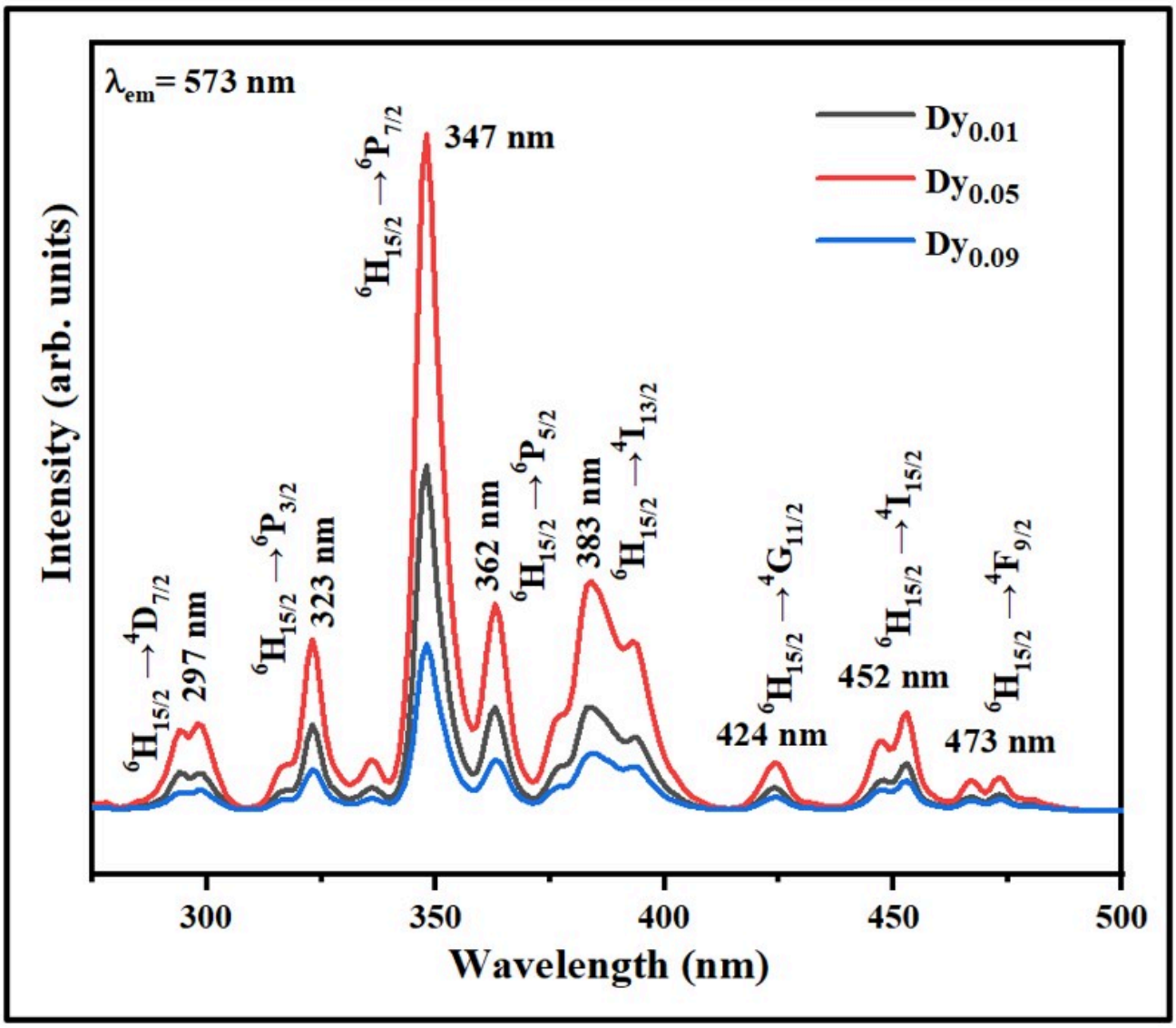


Figure 11

PLExcitation spectra of Dy^{3+} doped LCP NPs

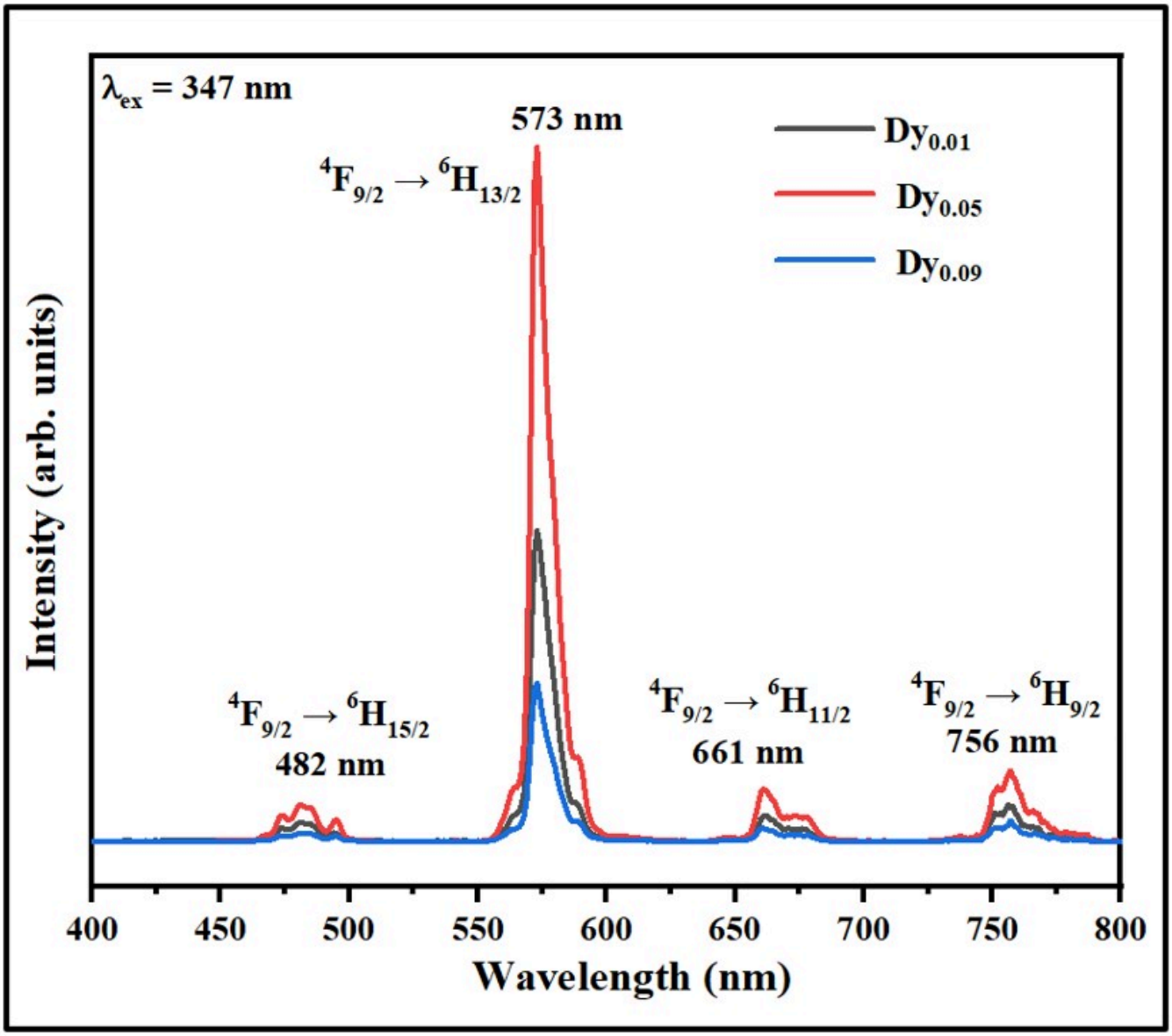


Figure 12

PL Emission spectra of Dy^{3+} doped LCP NPs

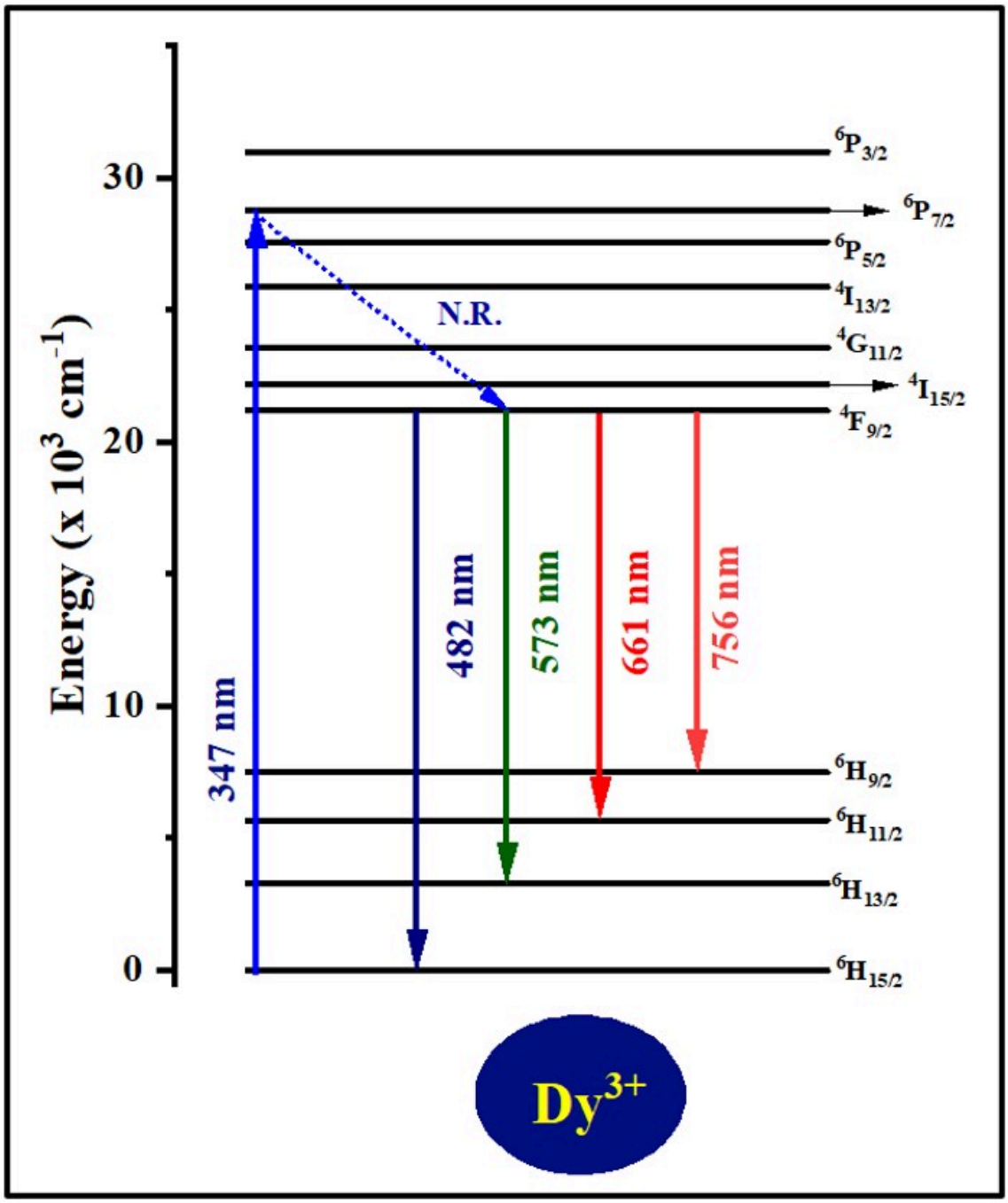


Figure 13

Energy level schematic diagram of Dy^{3+} ions in host system

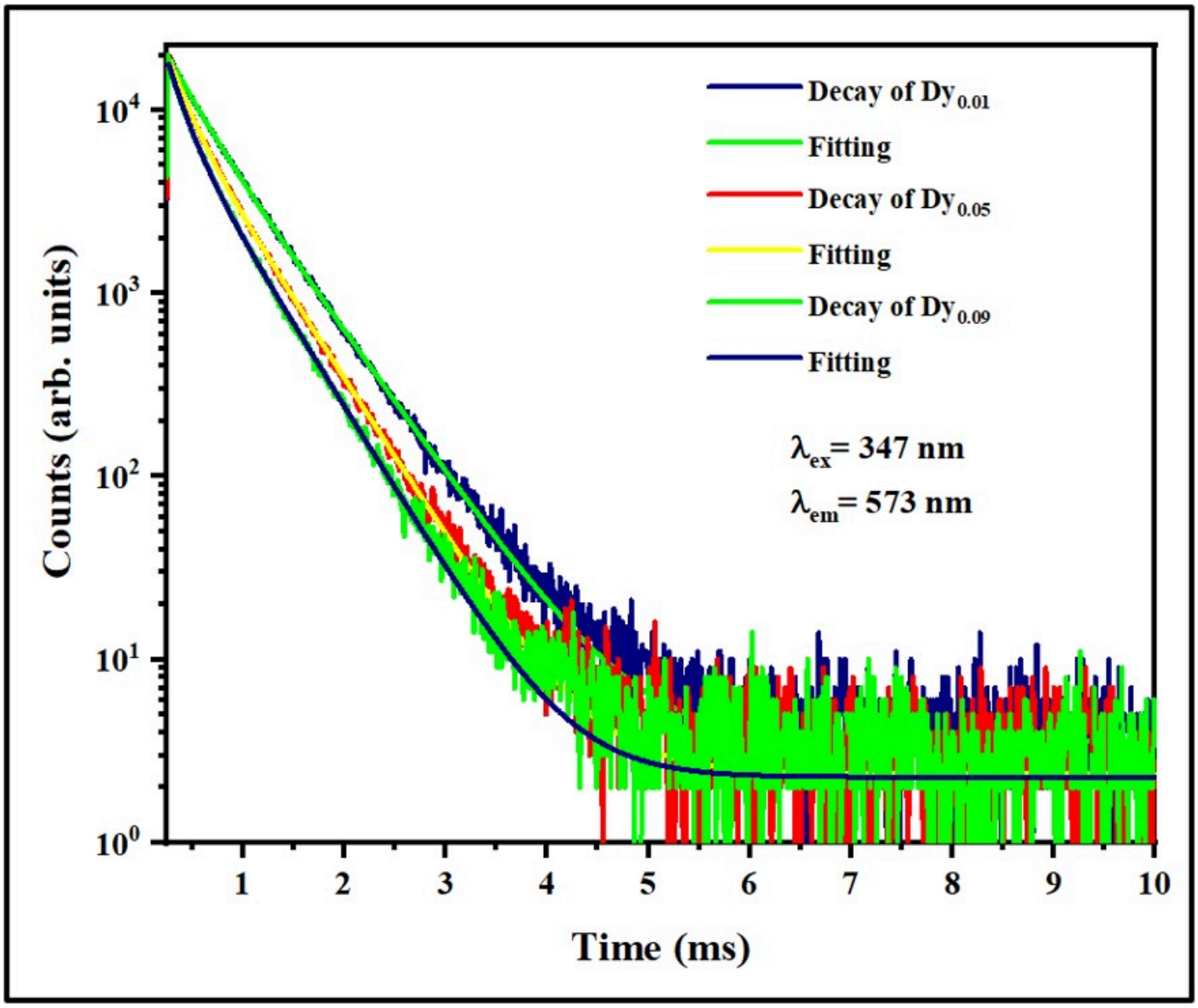


Figure 14

Lifetime decay curves of synthesizedLCP NPs

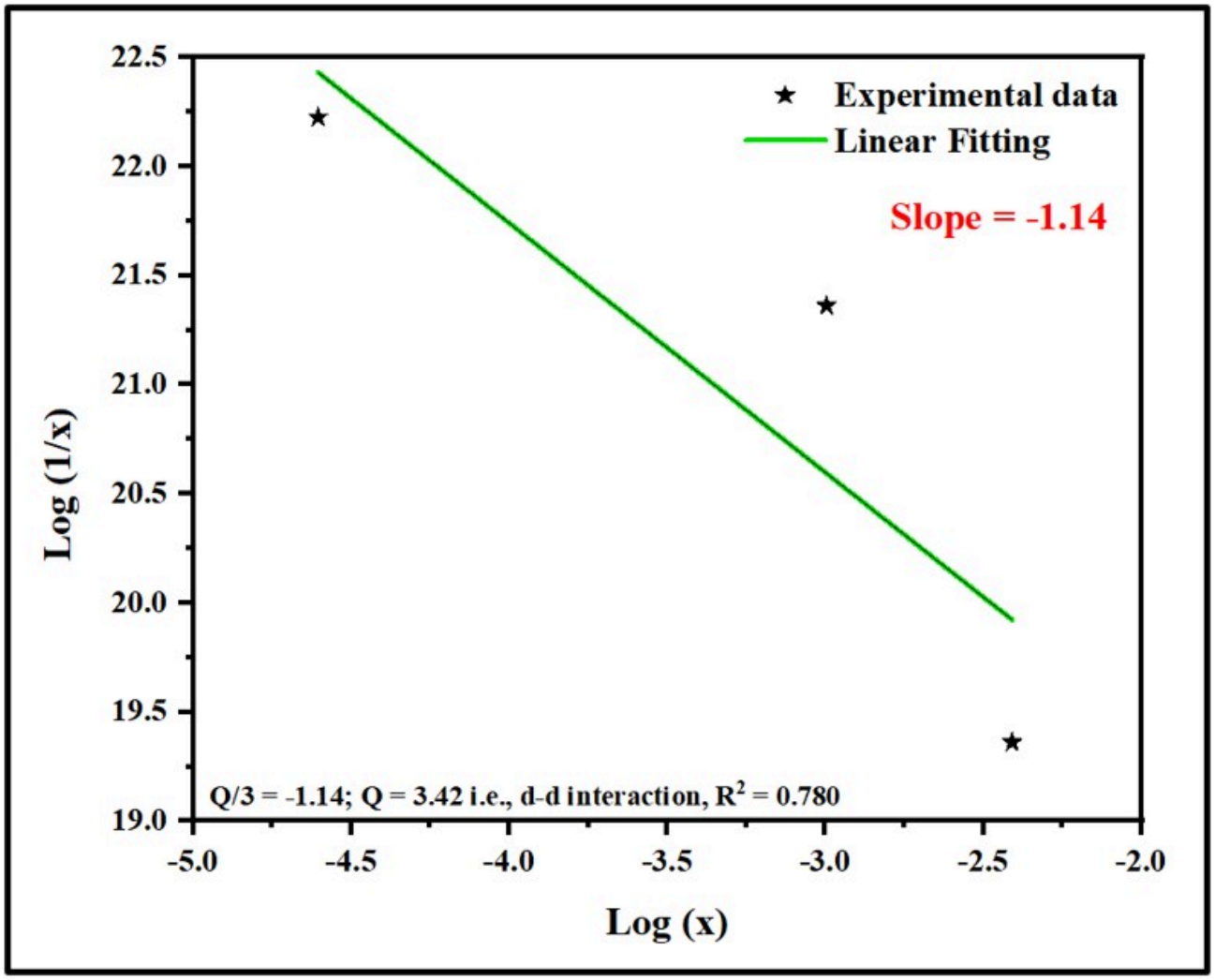


Figure 15

The fitting curve graph of log (I/x) - log (x) in Dy^{3+} doped LCP NPs

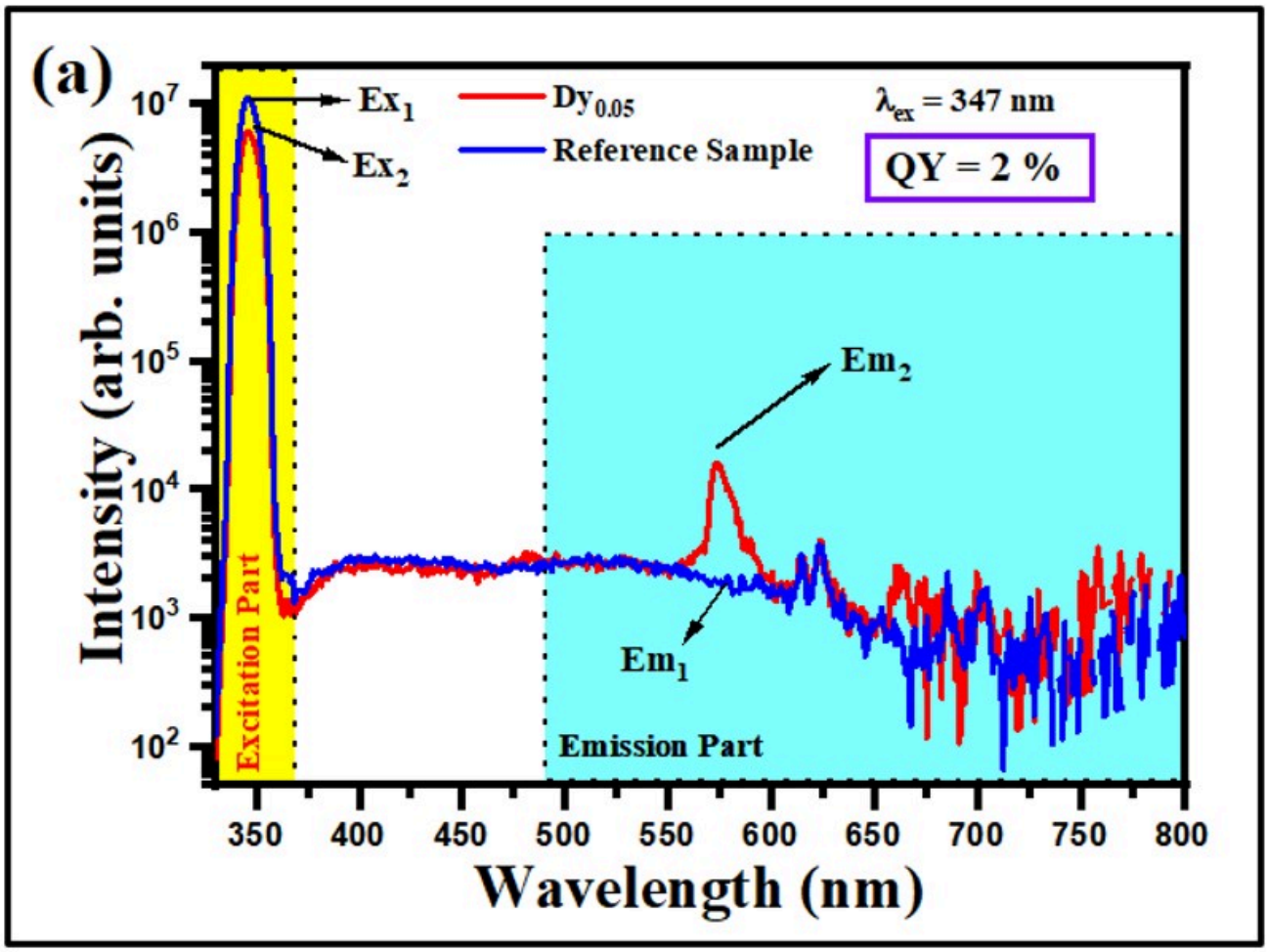


Figure 16

Photoluminescence quantum yield (PLQY) graphs of $Dy_{0.05}$sample for λ_{ex} = 347 nm

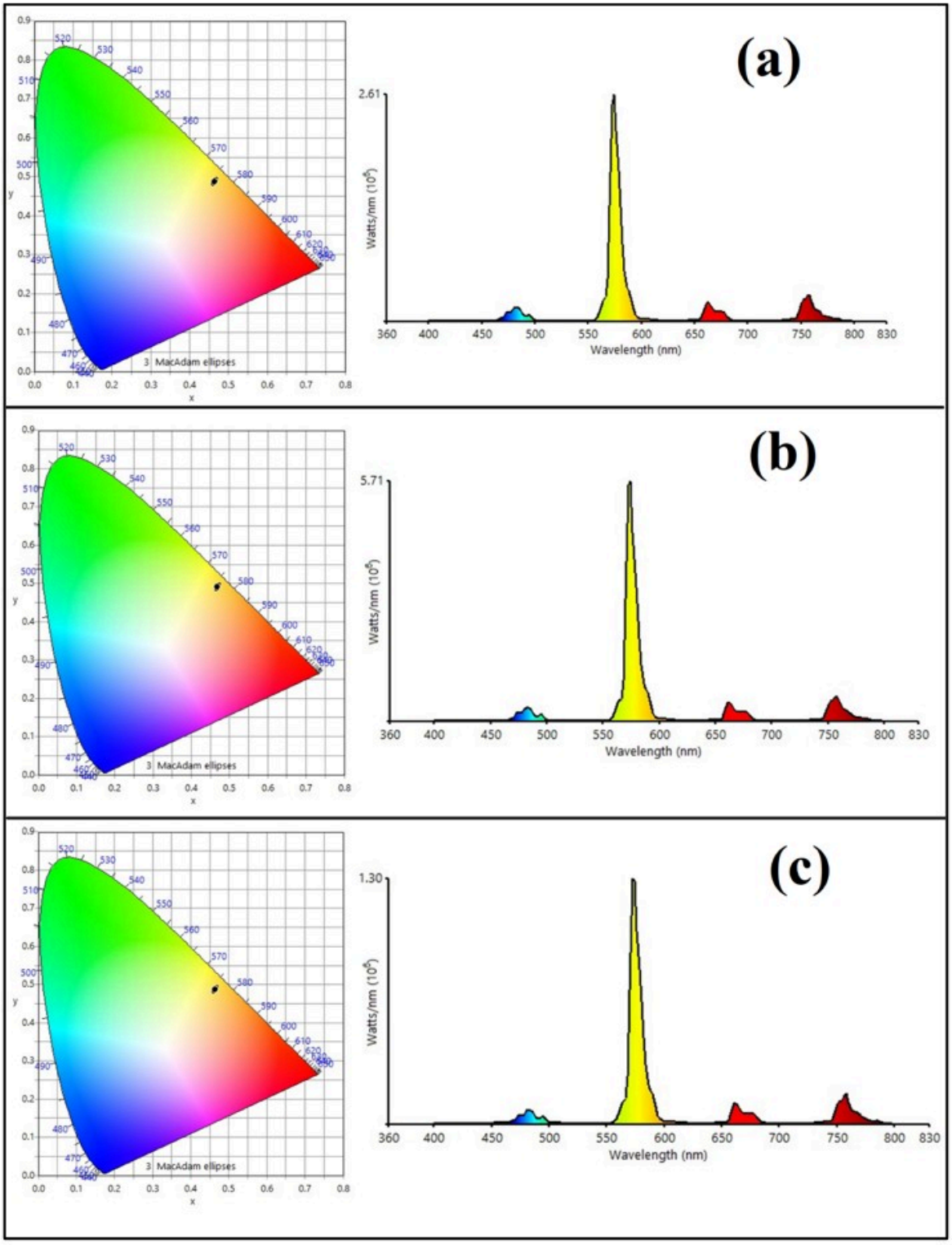


Figure 17

CIE chromaticity diagram of (a) Pure (b) $Dy_{0.01}$ (c) $Dy_{0.05}$and (d) $Dy_{0.09}$

Supplementary Files

This is a list of supplementary files associated with this preprint. Click to download.

- GraphicalAbstract.docx